AIP Publishing

This manuscript was accepted by Appl. Phys. Lett. Click here to see the version of record.

# Radiative recombination mechanisms in polar and non-polar InGaN/GaN quantum well LED structures

T. J. Badcock,[*1] M. Ali[1], T. Zhu[2], M. Pristovsek[2], R. A. Oliver[2] and A. J. Shields[1]

[1]*Toshiba Research Europe Ltd., Cambridge Research Laboratory, 208 Science Park, Milton Road, Cambridge, CB4 0GZ, United Kingdom*

[2]*Department of Materials Science and Metallurgy, 27 Charles Babbage Road, University of Cambridge, Cambridge, CB3 0FS, United Kingdom*

We study the photoluminescence internal quantum efficiency (IQE) and recombination dynamics in a pair of polar and non-polar InGaN/GaN quantum well (QW) light-emitting diode (LED) structures as a function of excess carrier density and temperature. In the polar LED at 293K, the variation of radiative and non-radiative lifetimes is well described by a modified ABC type model which accounts for the background carrier concentration in the QWs due to unintentional doping. As the temperature is reduced, the sensitivity of the radiative lifetime to excess carrier density becomes progressively weaker. We attribute this behaviour to the reduced mobility of the localised electrons and holes at low temperatures, resulting in a more monomolecular like radiative process. Thus we propose that in polar QWs, the degree of carrier localisation determines the sensitivity of the radiative lifetime to the excess carrier density. In the non-polar LED, the radiative lifetime is independent of excitation density at room temperature, consistent with a wholly excitonic recombination mechanism. These findings have significance for the interpretation of LED efficiency data within the context of the ABC recombination model.

ACCEPTED MANUSCRIPT

[*] e-mail: tjbadcock@yahoo.co.uk; current address: Oclaro Technology Ltd., Caswell, Towcester, NN12 8EQ, UK

AIP Publishing

This manuscript was accepted by Appl. Phys. Lett. Click here to see the version of record.

Studies relating to the internal quantum efficiency (IQE) of InGaN/GaN quantum well (QW) light-emitting diode (LED) structures are essential due to the huge market potential of these devices. Of particular interest is the phenomenon of "efficiency droop" – i.e. the reduction in efficiency at high drive current densities – since this is a major barrier to adoption[1]. It is well established that III-Nitride QWs grown in non- or semi-polar orientations possess greatly enhanced radiative recombination rates in comparison to their *c*-plane counterparts[2]. As a consequence, it is believed that droop will be alleviated or even eliminated in non-/semi-polar LEDs due to the fact that significantly reduced carrier densities can be obtained at a given injection current density. A widely used tool in the analysis of the experimentally measured light ($L$) vs. current density ($J$) dependence of all types of LEDs is the so-called ABC model[3]. In the model, the total recombination rate as a function of injected carrier density ($n$), $R(n) = An + Bn^2 + Cn^3$, where the coefficients $A$, $B$ and $C$ are associated with Shockley-Read-Hall, Radiative and Auger recombination respectively and the IQE $= Bn^2 / R(n)$. These definitions assume that the radiative recombination process is always in the majority carrier regime ($n \gg n_0$, $p_0$), where $n_0$, $p_0$ is the background concentration of electrons or holes in the QW. They also imply that the radiative process occurs only between completely uncorrelated electrons and holes, thus ignoring carrier localisation effects and the possibility of excitonic recombination[4]. In fact, when applied to InGaN/GaN LED $L$ – $J$ data, the extracted $C$ coefficient often may exceed theoretical estimations ($\sim10^{-31}$ cm$^6$s$^{-1}$) by two or three orders of magnitude[5], thus raising serious questions about the validity of the model. In order to consider other non-radiative processes as possible candidates for efficiency droop, additional terms relating to carrier leakage[6] and density activated defect recombination[7] have been included. Yet a universal feature of all ABC type models is that, within the injection regime well below the onset of droop, the IQE is assumed to be equal to $Bn^2 / (An + Bn^2)$. In this work we study the temperature dependent IQE and recombination dynamics as a function of photoexcitation density in polar and non-polar (*m*-plane) InGaN/GaN multiple QW LED structures containing nominally identical active regions. We show that the radiative recombination process is strongly affected by the growth orientation, background carrier concentration and the degree of carrier localisation, as determined by the temperature.

ACCEPTED MANUSCRIPT

AIP Publishing

This manuscript was accepted by Appl. Phys. Lett. Click here to see the version of record.

The polar and non-polar LED structures were grown by metal-organic vapour phase epitaxy. The polar *c*-plane sample was grown on a ~4 µm thick *n*-doped GaN template on 2-inch *c*-plane sapphire substrate with a low threading dislocation density of 3 x $10^8$ $cm^{-2}$. The non-polar sample was grown on free-standing *m*-plane GaN substrate (~5 x 10 $mm^2$) obtained from Kyma Technologies[8] with a miscut of 0.7° towards GaN [000-1] and a nominal dislocation density of <5 x $10^6$ $cm^{-2}$. Each LED structure contained 5 periods of 2.5 nm thick InGaN QWs separated by 7.5 nm thick GaN barriers grown using the 'Quasi two-temperature' methodology which results in continuous QWs free from gross QW width fluctuations[9]. The emission is centred around 450 nm and 470 nm in the polar and non-polar LEDs, respectively. The active region is clad by ~3 µm of Si-doped GaN ($N_d$ ~3 x $10^{18}$ $cm^{-3}$) and 130 nm of Mg doped GaN ($N_a$ ~3 x $10^{19}$ $cm^{-3}$). Electrically injected devices were fabricated using chlorine based inductively coupled plasma etching to form mesas with an area of 1.7 x $10^{-3}$ $cm^2$. A Ti/Al/Ti/Au metal stack annealed in $N_2$ ambient served as the *n*-type contact and a thin Ni/Au layer annealed in a mixture of $N_2/O_2$ was used as a semi-transparent current spreading layer on top of *p*-GaN.

For the photoluminescence (PL) measurements, pieces of unprocessed wafer were mounted on the cold finger of a continuous flow He microstat and excited by a switchable cw or pulsed (50 ps width, 5 MHz repetition rate) diode laser with a photon energy of 3.147 eV ($E_{las}$) which generates carriers directly in the QWs. The PL emission was focussed into a 0.64 m monochromator and detected by a cooled CCD array detector or a fast photosensor module for cw spectroscopy or PL decay measurements, respectively. The system response of the PL decay setup had a full-width at half maximum of 300 ps. All the PL decay data was acquired for a specified time period with the monochromator at zero-order in combination with high rejection long pass and short pass dielectric filters. This technique ensured that the resulting transient represented a spectral average of the QW emission, since it is well known that the recombination time in polar InGaN QWs varies across the luminescence linewidth[10-12]. The LED devices were probed on-chip and the electroluminescence (EL) emission was collected through the backside of the wafer into an integrating sphere equipped with a wavelength calibrated Si-photodiode. A LabVIEW routine controlled the $L – J$ sweep.

ACCEPTED MANUSCRIPT

AIP Publishing

This manuscript was accepted by Appl. Phys. Lett. Click here to see the version of record.

To verify the applicability of our PL technique for obtaining information on recombination processes in LEDs, we compare the excitation density dependence of the cw PL IQE and the EL IQE, for the polar LED at 293K, which is shown in Fig. 1. As standard, we define the PL IQE to be proportional to the integrated PL intensity per unit laser excitation power. This ratio is converted into IQE via a temperature dependent measurement of the PL intensity using a low excitation power with the usual assumption of 100% IQE at base temperature (6K). Since we do not know the extraction efficiency of our LEDs, we use the same temperature dependent methodology to determine the EL IQE. The PL measurements were made on unprocessed wafer (i.e. truly open circuit conditions) to eliminate the possibility of carrier escape via leakage to the contacts[13]. In Fig. 1, the optical and electrical excitation densities have been expressed in terms of a generation rate, $G_{Opt}$ = $(P_{las}.\alpha_{InGaN})/(A.E_{las})$ and $G_{Elec}$ $(=J/e.d)$ respectively, where $P_{las}$ is the laser excitation power, the excitation area ($A$) is measured to be ~ $10^{-8}$ $cm^{-2}$, the effective polar QW absorption coefficient ($\alpha_{InGaN}$) ~1 x $10^{4}$ $cm^{-1}$ (incorporating the predicted[14] reduction in optical matrix element due to the built-in fields across the QW) and $d$=2.5 nm (i.e the thickness of a single QW). $\alpha_{InGaN}$ is not expected to exhibit a strong variation with temperature at $E_{las}$ and so the photogeneration rate is taken to be temperature independent. It is apparent that the efficiency curves are very similar, regardless of whether the carriers are generated optically or electrically. The most obvious difference between the PL and EL data is the peak IQE, being ~10% higher in the latter case. In our methodology for determining the IQE, it is implicit that the carrier injection does not change with temperature. Whilst this is a reasonable assumption for quasi-resonant PL measurements in which the variation in $\alpha_{InGaN}$ at $E_{las}$ may be small, it cannot be assumed in the case of electrical injection. Indeed a reduction in injection efficiency due to drift induced carrier overspill with increasing forward bias is often cited as the cause of efficiency droop in InGaN/GaN LEDs[15]. However, given the occurrence of *photoluminescence* droop and its similarity to the EL efficiency curve, we do not believe this mechanism can account for the behaviour we observe at room temperature. Nevertheless, at low temperatures (< 100 K) where a large proportion of the hole concentration is frozen out, the asymmetry in electron and hole mobility will be exacerbated and the injection efficiency is likely to be reduced – an effect also compatible with the onset of droop at very low current densities (~$10^{-2}$ $A/cm^{2}$) at low temperatures[16]. Since our calculation of IQE relies on a temperature independent injection efficiency, this

ACCEPTED MANUSCRIPT

AIP Publishing
This manuscript was accepted by Appl. Phys. Lett. Click here to see the version of record.

therefore raises some doubt about the accuracy of our EL IQE determination and potentially produces a slightly exaggerated EL IQE at room temperature, as borne out by the data in Fig. 1. Unfortunately the same approach for comparing the PL and EL in the *m*-plane LED could not be adopted, due to the low hole conductivity of the *p*-GaN which resulted in spatially non-uniform emission and prevented accurate estimation of the electrically injected area. However, the cw PL IQE of the *m*-plane LED is plotted in Fig. 1, showing similar characteristics to the pulsed behaviour discussed below (Fig. 2 (b)). In evaluating $G_{Opt}$, $\alpha_{InGaN}$ is estimated to be 1 x $10^5$ $cm^{-1}$ and a longer focal length focussing lens is used, resulting in rather similar range of $G_{Opt}$ values for both polar and non-polar LEDs.

Shown in Fig. 2(a) and (b) is a comparison of the pulsed PL IQE for the polar and non-polar LED structures, at various temperatures between 6K and 293K. The integrated PL intensity is obtained by temporally integrating individual PL transients. As in the cw case, the IQE is derived from a normalisation to the 6K data under low injection conditions. The assumption of 100% IQE at 6K is supported by the observation of similar (within 50%) *absolute PL intensities* in the polar and non-polar samples at 293K for a carrier density ~$10^{18}$ $cm^{-3}$. At 6K, the IQE is approximately independent of excitation density for both samples. With increasing temperature however, the peak IQE of the polar LED reduces and the emission intensity develops a strongly superlinear dependence on excitation density. In contrast, for the non-polar device, *the IQE remains independent of excitation density* across a wide range of excitation densities, both at 6K and 293K. We point out here that the reduction of the 293K IQE in the non-polar sample at the highest excitation densities is due to the onset of droop, as observed recently by Davies *et al.*[17] at cryogenic temperatures. The behaviour exhibited by the polar LED is consistent with the thermally activated onset of a competing non-radiative process in conjunction with a radiative mechanism possessing a higher-order carrier density dependence, generally taken[18] to be $\propto n^2$. In the case of the non-polar sample, the reduction in IQE at 293K is not accompanied by a change in the excitation dependence of the IQE, suggesting that competition between radiative and non-radiative processes in this sample is qualitatively different.

To investigate the origin of these differences in the efficiency behaviour between polar and non-polar samples, we now compare the excitation dependence of the recombination dynamics in each structure at 6K and



ACCEPTED MANUSCRIPT

AIP Publishing
This manuscript was accepted by Appl. Phys. Lett. Click here to see the version of record.

293K as shown in Fig. 3. In our experiment, the radiative and non-radiative carrier lifetimes are related to the IQE in the conventional manner for parallel decay channels. Thus, the temperature ($T$) and carrier density ($\Delta n$) dependent radiative lifetime $\tau_{rad}(T,\Delta n) = \tau_m(T,\Delta n)$/IQE, where we choose $\tau_m(T,\Delta n)$ to be the measured time interval in which the PL signal decays to $e^{-1}$ of its maximum, initial value. Likewise, the non-radiative lifetime $\tau_{non\text{-}rad}(T,\Delta n) = \tau_m(T,\Delta n).\tau_{rad}(T,\Delta n)/[\tau_{rad}(T,\Delta n) - \tau_m(T,\Delta n)]$. Although it is not strictly valid to characterise non-exponential decays, such as those in Fig. 3, by $e^{-1}$ time constants, we believe the approximation is justified based on the close agreement we observe between the theoretically predicted and experimentally determined variations of $\tau_{rad}$ and $\tau_{non\text{-}rad}$ (see Fig. 5(a)). In line with other recent reports on the optical properties of non-polar InGaN/GaN QWs[19,12] we find that the 6K PL transients in the non-polar LED (see Fig. 4) decay exponentially with a sub-ns timescale ($\tau_{rad}$ ~460 ps) that does not vary across the lineshape: properties that are attributable to the absence of the built-in electric field[12]. At 6K, the PL transients of both the non-polar and the polar LED are independent of excitation density over a wide range[20], consistent with the dominance of radiative recombination and unity IQE.

At 293K however, where non-radiative processes compete more strongly, the behaviours of the samples diverge strongly. In the polar LED, the decay lengthens with increasing excitation density up to excitation levels of ~$10^{18}$ $cm^{-3}$ (see Fig. 3). Taken together with the progressive increase in IQE over the same excitation range (see Fig. 2 (a)), this observation suggests that the proportional increase in non-radiative lifetime is much more than any corresponding decrease in the radiative lifetime due to bimolecular recombination, contrary to the interpretation provided by simple ABC models. In the non-polar LED however, $\tau_{rad}(T,\Delta n)$ remains independent of excitation at 293K and is only very weakly temperature dependent – reaching ~960 ps at 293K.

As is well established, the absence of the macroscopic polarisation fields in non-polar (In)(Al)GaN/GaN QWs results in greatly enhanced radiative recombination rates due to the increased overlap of the electron and hole envelope functions. A second, often overlooked, consequence of the increased overlap is the stronger Coulomb interaction between electrons and holes which enhances the exciton binding energy[19]. Exciton binding energies in excess of 60 meV have been calculated[19] and measured[21] in similar non-polar (In)GaN and GaN QW structures

ACCEPTED MANUSCRIPT

AIP Publishing

This manuscript was accepted by Appl. Phys. Lett. Click here to see the version of record.

respectively, and so it is highly probable that the room temperature emission in the non-polar LED is dominated by the recombination of excitons. Indeed an excitonic radiative process in competition with SRH recombination in the minority carrier regime ($\Delta n < n_0$) would produce the excitation invariant IQE we observe at room temperature (see Fig. 2(b)). Furthermore, the small increase in $\tau_{rad}(T,\Delta n)$ between 6K and 293K in the non-polar LED implies that the room temperature emission originates from the recombination of strongly localised excitons[22+phil 23].

Although carrier localisation effects are also significant for polar QWs, there is now an increasing body of theoretical and experimental evidence that points to a difference in the nature of the carrier localisation mechanism for polar and non-polar QWs. Atomistic modelling of the potential energy landscape in InGaN QWs has revealed that the localised electron and hole wavefunctions in polar $In_xGa_{1-x}N$/GaN QWs (x~0.17) are not spatially correlated, even accounting for the Coulomb interaction, due to the combined effects of alloy disorder and the macroscopic polarisation field discontinuity across the QW. The built-in electric field inherent to polar QWs results in separate localisation mechanisms for electrons and holes[24]; holes being localised by random alloy disorder while electrons localise predominately at monolayer QW width fluctuations[25]. As can be seen in Fig. 5(a): at 293K, $\tau_{rad}(T,\Delta n)$ in the polar LED is approximately independent of $\Delta n$ for excitation < ~$10^{17}$ cm$^{-3}$ whereas $\tau_{non\text{-}rad}(T,\Delta n)$ increases by a factor of ~6, validating our claim that at low excitation densities ($\Delta n \leq n_0$, where $n_0$ is the background concentration of free electrons) it is primarily changes in $\tau_{non\text{-}rad}(T,\Delta n)$ which determine the IQE. Non-radiative recombination in this low density regime is generally treated by the SRH theory of non-radiative recombination at a deep centre[26]. The carrier lifetime associated with SRH recombination $\tau_{non\text{-}rad}(T,\Delta n) = \tau_{p0} + \tau_{n0}[\Delta n/(\Delta n + n_0)]$, where $\tau_{p0}$ and $\tau_{n0}$ are the lifetimes of holes and electrons under the assumption that all SRH recombination centres are occupied by electrons or holes, respectively. In the ABC model, the $A$ coefficient corresponds to the case where $\Delta n >> n_0$ and thus $A^{-1} = \tau_{p0} + \tau_{n0}$, which is independent of $\Delta n$. The $\tau_{non\text{-}rad}(T,\Delta n)$ data of Fig. 5(a) can be fitted over the range $10^{16} < \Delta n < 10^{18}$ cm$^{-3}$ with the SRH equation using $n_0 = 4 \times 10^{17}$ cm$^{-3}$, $\tau_{p0} = 0.8$ ns and $\tau_{n0} = 20$ ns (see green dashed line). Note that we do not assume the maximum experimentally determined value of $\tau_{non\text{-}rad}(T,\Delta n)$ (~12 ns) necessarily corresponds to the high injection lifetime $\tau_{p0} + \tau_{n0}$, since a

ACCEPTED MANUSCRIPT

AIP Publishing

This manuscript was accepted by Appl. Phys. Lett. Click here to see the version of record.

second non-radiative process that is related to droop will become increasingly competitive at these carrier densities. Indeed the reduction in $\tau_{non\text{-}rad}(T,\Delta n)$ we observe above ~$10^{18}$ cm$^{-3}$ is correlated with the emergence of an initial, fast, component in the PL transient (see 6.5 x $10^{18}$ cm$^{-3}$ transient in Fig. 3) and is likely to indicate the onset of a higher-order non-radiative process connected with efficiency droop, possibly due to Auger[27] or carrier delocalisation[7, 20].

The presence of a significant background carrier concentration also affects the radiative recombination rate[28]. Now, $\tau_{rad}(T,\Delta n) = (B[n_0 + \Delta n])^{-1}$ instead of $(B.\Delta n)^{-1}$, as would be the case for purely bimolecular radiative recombination. This dependence ($\tau_{rad\text{-}theory}$) is plotted in Fig. 5(a), with $n_0 = 4 \times 10^{17}$ cm$^{-3}$ and $B = 1.5 \times 10^{-11}$ cm$^3$s$^{-1}$. The agreement with experimental data is fairly good, suggesting that it is essential to consider the magnitude of the background doping when applying the ABC model (i.e. it is generally invalid to assume $\Delta n >> n_0$). We point out here that the PL peak energy remains, within experimental error (±5 meV), approximately constant throughout the investigated excitation range and so photo-carrier induced screening of the built-in fields across the QW cannot account for the significant reduction we observe in $\tau_{rad}(T,\Delta n)$. Although this straightforward adaptation of the radiative and SRH terms is able to describe room temperature data, it does not seem to be applicable at lower temperatures. As shown in Fig 5(b), the excess carrier density dependence of $\tau_{rad}(T,\Delta n)$ becomes weaker as the temperature is decreased. Within the context of the discussion above, this behaviour can only be accounted for by assuming that the background doping concentration in the QW increases with reducing temperature, a process which is physically implausible. A more reasonable explanation involves a consideration of carrier localisation. At the lowest temperatures, the radiative recombination occurs between immobile populations of spatially localised electrons and holes[24] which nevertheless possess a high degree of correlation due to the localised nature of the recombination site. This results in a radiative recombination rate which is independent of excess carrier density. As the temperature increases, the carriers become more mobile and are able to escape to neighbouring localisation sites via acoustic phonon scattering. This process effectively reduces the degree of spatial correlation between the electrons and holes and causes the rate of radiative recombination to become a product of their respective densities[29]. Crucially, it is the uncorrelated nature of the electron and hole localisation and transport in polar QWs which in effect mimics the classic $Bn^2$ description, even though the mechanism we describe does not

ACCEPTED MANUSCRIPT

AIP Publishing

This manuscript was accepted by Appl. Phys. Lett. Click here to see the version of record.

involve 'free' carriers moving in 'bands'. It is likely that details of the carrier localisation environment (e.g. the density of localised states) in polar InGaN QWs have a significant influence on the extent of the electron-hole correlation for a given temperature. For example, in wide, smooth QWs with small carrier localisation energies and Coulomb interaction energies the $Bn^2$ limit will be approached most closely. Whereas in narrower QWs, with deeper localisation and stronger Coulombic effects, it is more appropriate to adopt an excitonic picture for the radiative process.

In summary, we have shown that the radiative recombination mechanism in polar and non-polar InGaN/GaN LED structures is fundamentally different. Non-polar LEDs are dominated by excitonic recombination at room temperature. Whereas in polar LEDs the uncorrelated nature of the electron-hole localisation results in a carrier density dependent radiative lifetime which can be described by an ABC-type model that includes the background carrier concentration. Our inference that it is invalid to assume a universally applicable radiative recombination rate ($=Bn^2$) when analysing LED EQE data may help shed some light on the variety of reported $A$, $B$ and $C$ parameters[5] obtained from nominally similar LED structures.

**References**


1. G. Verzellesi, D. Saguatti, M. Meneghini, F. Bertazzi, M. Goano, G. Meneghesso and E. Zanoni, J. Appl. Phys. **114**, 071101 (2013); J. Cho, E. F. Schubert and J .K. Kim, Laser & Photon. Rev., **7**, 3, 408 (2013)
2. P. Waltereit, O. Brandt, A. Trampert, H. T. Grahn, J. Menniger, M. Ramsteiner, M. Reiche and K. H. Ploog, Nature **406**, 865 (2000).
3. S. Y. Karpov Optical and Quantum Electronics **47** (6) 1293 (2015).
4. T. Langer, A. Chernikov, D. Kalincev, M. Gerhard, H. Bremers, U. Rossow, M. Koch and A. Hangleiter, Appl. Phys. Lett. **103**, 202106 (2013).
5. J. Piprek, F. Römer and B. Witzigmann Appl. Phys. Lett. **106**, 101101 (2015).
6. D. S. Meyaard, G.-B. Lin, J. Cho, E. F. Schubert, H. Shim, S.-H. Han, M.-H. Kim, C. Sone and Y. S. Kim, Appl. Phys. Lett. **102**, 251114 (2013).
7. J. Hader, J. V. Moloney and S. W. Koch, Appl. Phys. Lett. **96**, 221106 (2010).


ACCEPTED MANUSCRIPT

AIP Publishing

This manuscript was accepted by Appl. Phys. Lett. Click here to see the version of record.

ACCEPTED MANUSCRIPT


8. D. Hanser, L. Liu, E. A. Preble, K. Udwary, T. Paskova, and K. R. Evans, J. Cryst. Growth **310**, 3953 (2008).
9. R. A. Oliver, J. Sumner, M. J. Kappers and C. J. Humphreys, J. Appl. Phys. **106**, 054319 (2009).
10. T. J. Badcock, P. Dawson, M. J. Davies, M. J. Kappers, F. C.-P. Massabuau, F. Oehler, R. A. Oliver and C. J. Humphreys, J. Appl. Phys. **115**, 113505 (2014).
11. A. Morel, P. Lefebvre, S. Kalliakos, T. Taliercio, T. Bretagnon and B. Gil, Phys. Rev. B **68**, 045331 (2003).
12. T. Langer, H.-G. Pietscher, F. A. Ketzer, H. Jönen, H. Bremers, U. Rossow, D. Menzel and A. Hangleiter, Phys. Rev. B **90**, 205302 (2014).
13. M. F. Schubert, Q. Dai, J. Xu, J. K. Kim and E. F. Schubert, Appl. Phys. Lett. **95**, 191105 (2009).
14. Based on simulations performed using SiLENSe software (http://www.str-soft.com/products/SiLENSe/#SiLENSe)
15. G.-B. Lin, D. Meyaard, J. Cho, E. F. Schubert, H. Shim and C. Sone, Appl. Phys Lett. **100**, 161106 (2012).
16. K.-S. Kim, D.-P. Han, H.-S. Kim and J.-I. Shim, Appl. Phys. Lett. **104**, 091110 (2014).
17. M. J. Davies, P. Dawson, S. Hammersley, T. Zhu, M. J. Kappers, C. J. Humphreys and R. A. Oliver, Appl. Phys. Lett. **108**, 252101 (2016).
18. B. Sermage, F. Alexandre, J. Beerens and P. Tronc, Superlatt. and Micros. **6**, (4), 373 (1989).
19. S. Schulz, D. P. Tanner, E. P. O'Reilly, M. A. Caro, T. L. Martin, P. A. J. Bagot, M. P. Moody, F. Tang, J. T. Griffiths, F. Oehler, M. J. Kappers, R. A. Oliver, C. J. Humphreys, D. Sutherland, M. J. Davies and P. Dawson, Phys. Rev. B **92**, 235419 (2015).
20. M. J. Davies, T. J. Badcock, P. Dawson, M. J. Kappers, R. A. Oliver and C. J. Humphreys, Appl. Phys. Lett. **102**, 022106 (2013).
21. T. J. Badcock, P. Dawson, M. J. Kappers, C. McAleese, J. L. Hollander, C. F. Johnston, D. V. Sridhara Rao, A. M. Sanchez and C. J. Humphreys, J. Appl. Phys. **105**, 123112 (2009).
22. D. S. Citrin, Phys. Rev. B **47**, 3832 (1993).

AIP Publishing

This manuscript was accepted by Appl. Phys. Lett. Click here to see the version of record.

23. P. Dawson, S. Schulz, R. A. Oliver, M. J. Kappers and C. J. Humphreys, J. Appl. Phys. **119**, 181505 (2016).

24. D. Watson-Parris, M. J. Godfrey, P. Dawson, R. A. Oliver, M. J. Galtrey, M. J. Kappers and C. J. Humphreys, Phys. Rev. B **83**, 115321 (2011).

25. S. Schulz, M. A. Caro, C. Coughlan, and E. P. O'Reilly, Phys. Rev. B **91**, 035439 (2015).

26. D. Macdonald and A. Cuevas, Phys. Rev. B **67**, 075203 (2003).

27. K. W. Williams, N. R. Monahan, D. D. Koleske, M. H. Crawford and X.-Y. Zhu, Appl. Phys. Lett. **108**, 141105 (2016).

28. B. Galler, H.-J. Lugauer, M. Binder, R. Hollweck, Y. Folwill, A. Nirschl, A. Gomez-Iglesias, B. Hahn, J. Wagner and M. Sabathil, Appl. Phys. Exp. **6**, 112101 (2013).

29. E. C. Le Ru, J. Fack and R. Murray, Phys Rev. B **67**, 245318 (2003); P. Dawson, O. Rubel, D. Baranovskii, K. Pierz, P. Thomas and E. O. Göbel, *ibid* **72**, 235301 (2005).

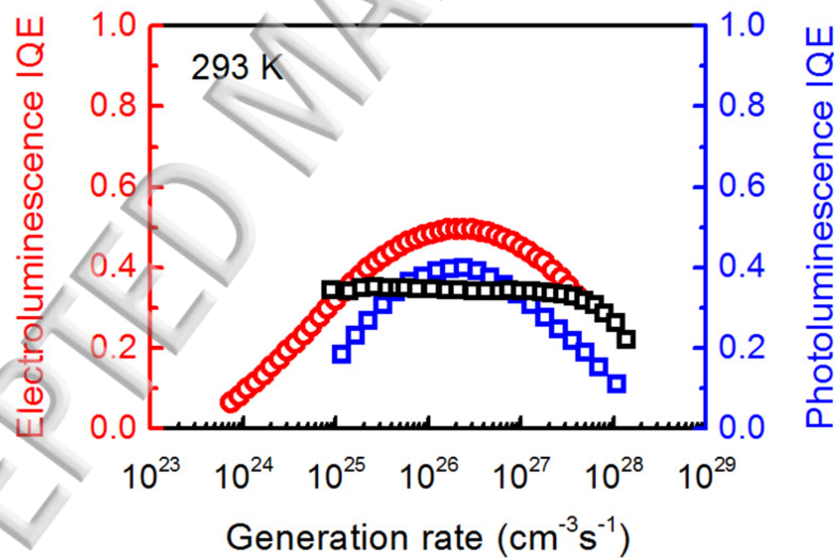


FIG. 1. Electroluminescence IQE (open red circles – left axis) and cw PL IQE (open blue squares – right axis) of the polar LED structure at room temperature. The cw PL IQE of the non-polar LED is also shown (open black squares).

ACCEPTED MANUSCRIPT

AIP Publishing

This manuscript was accepted by Appl. Phys. Lett. Click here to see the version of record.

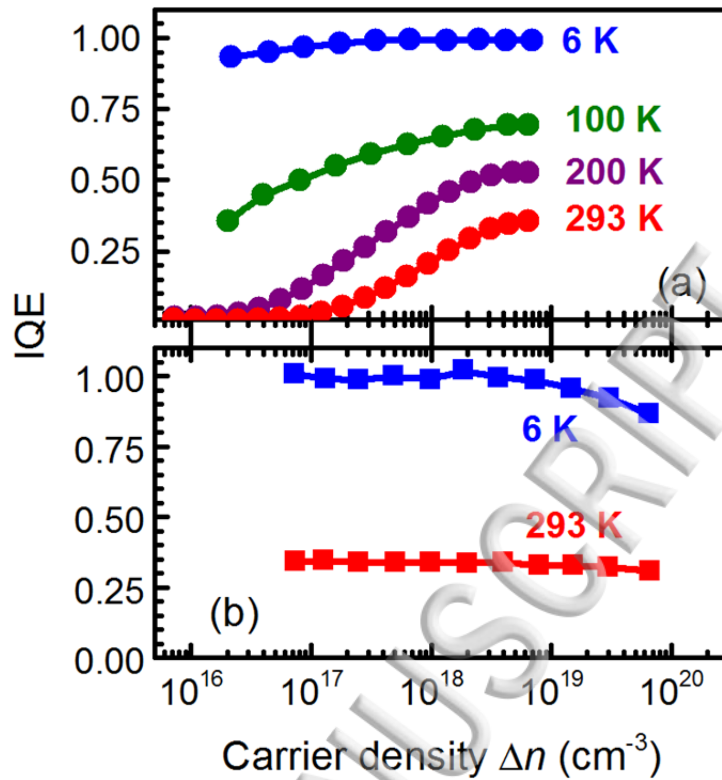


FIG. 2. PL IQE of the polar LED (a) and non-polar LED (b), acquired under pulsed excitation at various temperatures (indicated in figure).

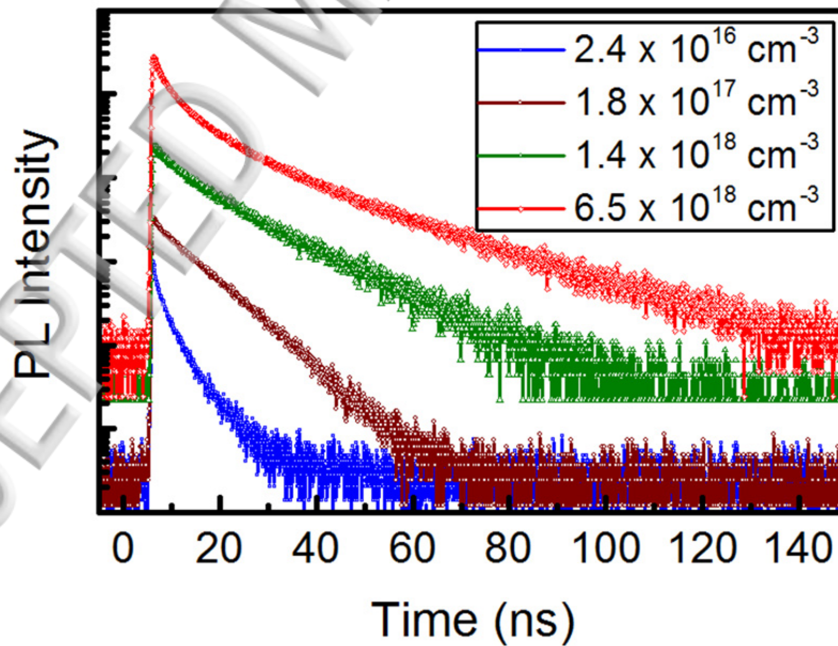


FIG. 3. Spectrally integrated PL transients for the polar LED at 293K, acquired at different excess carrier densities.

ACCEPTED MANUSCRIPT

AIP Publishing

This manuscript was accepted by Appl. Phys. Lett. Click here to see the version of record.

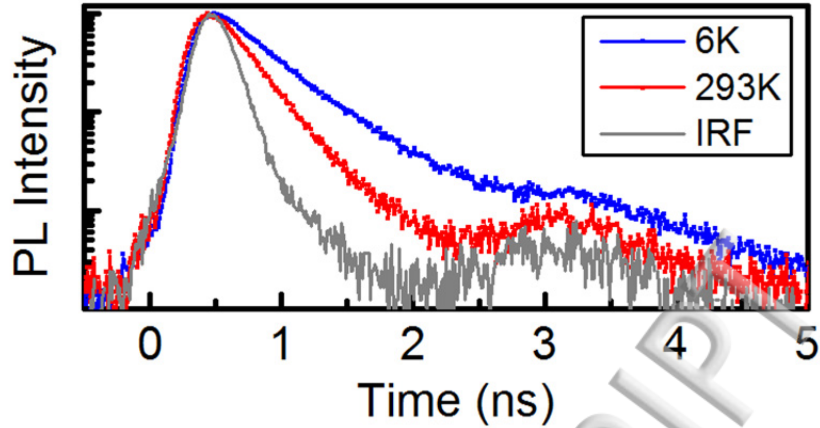


FIG. 4. Spectrally integrated PL transients for the non-polar LED at 6K and 293K, acquired at an excess carrier density of ~5x10$^{17}$ cm$^{-3}$. At 293K, $\tau_{rad}$ and $\tau_{non\text{-}rad}$ are 960 ps and 530 ps, respectively. The system response (IRF) is also shown.

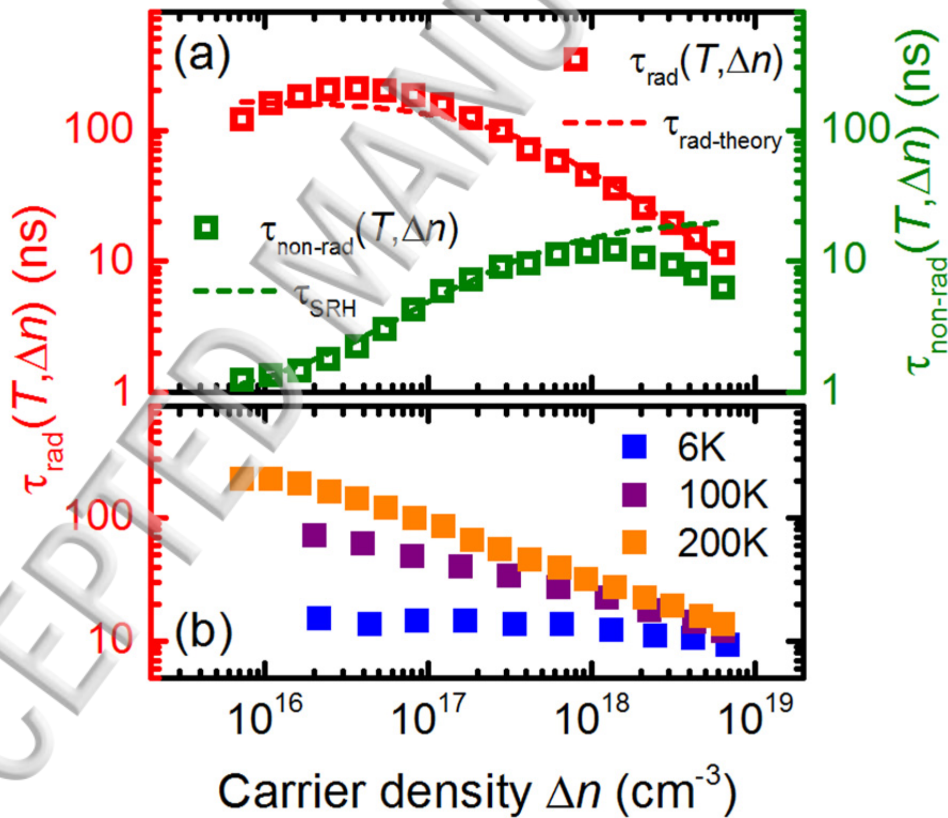


FIG. 5. (a) Measured radiative lifetime (open red squares – left axis) and non-radiative lifetime (open green squares – right axis) as a function of carrier density for the polar LED at 293K. The dashed red and green lines denote the theoretical radiative and non-radiative lifetimes, respectively; (b) measured radiative lifetime as a function of carrier density at 7K, 100K and 200K.

ACCEPTED MANUSCRIPT

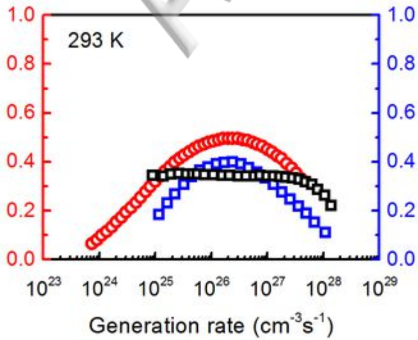
Electroluminescence IQE
Photoluminescence IQE
293 K
1.0
0.8
0.6
0.4
0.2
0.0
$10^{23}$
$10^{24}$
$10^{25}$
$10^{26}$
$10^{27}$
$10^{28}$
$10^{29}$
Generation rate ($cm^{-3}s^{-1}$)

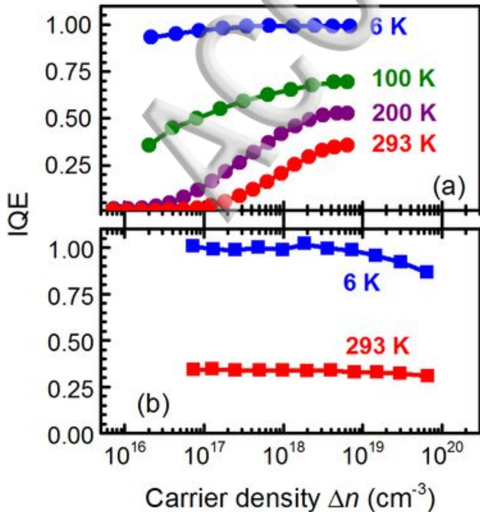

1.00
0.75
0.50
0.25
6 K
100 K
200 K
293 K
(a)
IQE
1.00
0.75
0.50
0.25
0.00
6 K
293 K
(b)
$10^{16}$
$10^{17}$
$10^{18}$
$10^{19}$
$10^{20}$
Carrier density $\Delta n$ (cm$^{-3}$)

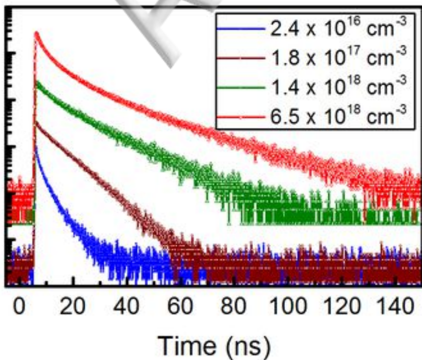
PL Intensity
Time (ns)
0
20
40
60
80
100
120
140
2.4 x $10^{16}$ cm$^{-3}$
1.8 x $10^{17}$ cm$^{-3}$
1.4 x $10^{18}$ cm$^{-3}$
6.5 x $10^{18}$ cm$^{-3}$

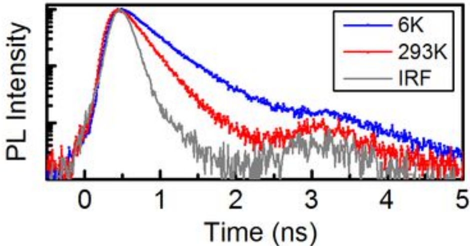

PL Intensity
Time (ns)
0
1
2
3
4
5
6K
293K
IRF

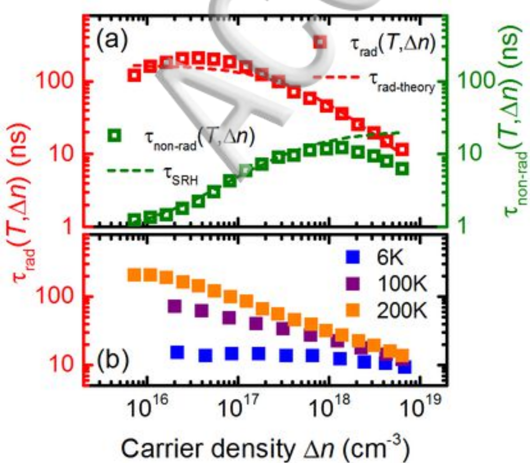
(a)
$\tau_{rad}(T,\Delta n)$
$\tau_{rad\text{-}theory}$
$\tau_{non\text{-}rad}(T,\Delta n)$
$\tau_{SRH}$
$\tau_{rad}(T,\Delta n)$ (ns)
$\tau_{non\text{-}rad}(T,\Delta n)$ (ns)
100
10
1
(b)
6K
100K
200K
$10^{16}$
$10^{17}$
$10^{18}$
$10^{19}$
Carrier density $\Delta n$ ($cm^{-3}$)